Non-linear dynamics

Phenomenology, applications and examples

Yannis PAPAPHILIPPOU
Accelerator and Beam Physics group
Beams Department
CERN

CERN Accelerator School
Advanced Accelerator Physics Course 2015
Warsaw, Poland
2-3 October 2015

Summary of the 1st lecture

- **Hamiltonian formalism** provides the **natural framework** to analyse (linear and non-linear) beam dynamics
- **Canonical (symplectic) transformations** enable to move from variables describing a distorted phase space to something simpler (ideally circles)
- The **generating functions** passing from the old to the new variables are bounded to **diverge** in the vicinity of **resonances** (emergence of chaos, see 2nd lecture)
- Calculating this generating function with **canonical perturbation theory** becomes **hopeless** for higher orders
- Representing the accelerator (or beam line) like a composition of maps (through **Lie transformations**) enables derivation of the generating functions in an **algorithmic way**, in principle to **arbitrary order**

Phase space dynamics - Fixed point analysis

Phase space dynamics

- Valuable description when examining trajectories in **phase space** (u, p_u)
- Existence of integral of motion imposes geometrical constraints on phase flow
- For the simple **harmonic oscillator**

$$H = \frac{1}{2}\left(p_u^2 + \omega_0^2 u^2\right)$$

  phase space curves are **ellipses** around the equilibrium point parameterized by the integral of motion Hamiltonian (energy)
- By simply **changing** the **sign** of the potential in the harmonic oscillator, the phase trajectories become **hyperbolas**, symmetric around the equilibrium point where two straight lines cross, moving towards and away from it

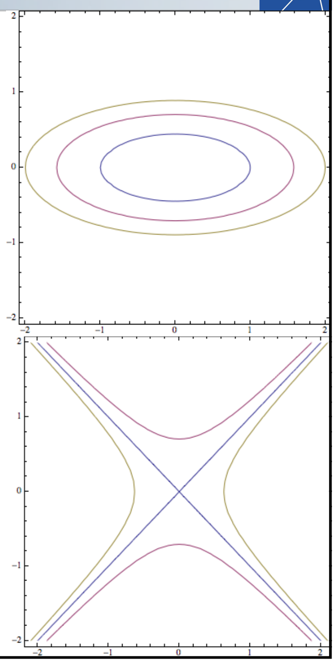

Non-linear oscillators

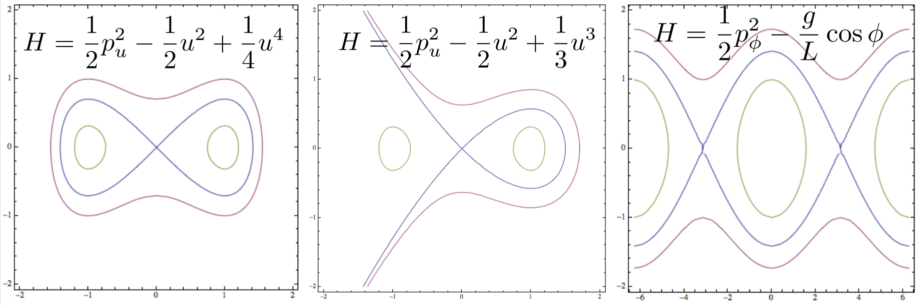

- Conservative non-linear oscillators have Hamiltonian

$$H = E = \frac{1}{2}p_u^2 + V(u)$$

with the potential being a general (polynomial) function of positions

- **Equilibrium points** are associated with extrema of the potential
- Considering three non-linear oscillators
  - **Quartic** potential (left): two minima and one maximum
  - **Cubic** potential (center): one minimum and one maximum
  - **Pendulum** (right): periodic minima and maxima

Fixed point analysis

- Consider a general second order system

$$\begin{aligned} \frac{du}{dt} &= f_1(u, p_u) \\ \frac{dp_u}{dt} &= f_2(u, p_u) \end{aligned}$$

- **Equilibrium** or "**fixed**" points $f_1(u_0, p_{u0}) = f_2(u_0, p_{u0}) = 0$ are determinant for topology of trajectories at their vicinity
- The linearized equations of motion at their vicinity are

$$\frac{d}{dt}\begin{bmatrix}\delta u \\ \delta p_u\end{bmatrix} = \mathcal{M}_J \begin{bmatrix}\delta u \\ \delta p_u\end{bmatrix} = \underbrace{\begin{bmatrix} \frac{\partial f_1(u_0, p_{u0})}{\partial u} & \frac{\partial f_1(u_0, p_{u0})}{\partial p_u} \\ \frac{\partial f_2(u_0, p_{u0})}{\partial u} & \frac{\partial f_2(u_0, p_{u0})}{\partial p_u} \end{bmatrix}}_{\textbf{Jacobian}\text{ matrix}} \begin{bmatrix}\delta u \\ \delta p_u\end{bmatrix}$$

- Fixed point nature is revealed by eigenvalues of $\mathcal{M}_J$, i.e. solutions of the characteristic polynomial $\det|\mathcal{M}_J - \lambda\mathbf{I}| = 0$

Fixed point for conservative systems

- For conservative systems of 1 degree of freedom, the second order characteristic polynomial has two solutions:
  - Two **complex eigenvalues** with opposite sign, corresponding to **elliptic** fixed points. Phase space flow is described by **ellipses**, with particles evolving clockwise or anti-clockwise
  - Two **real eigenvalues** with opposite sign, corresponding to **hyperbolic** (or saddle) fixed points. Flow described by two lines (or manifolds), incoming (stable) and outcoming (unstable)

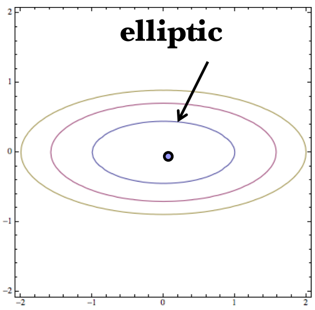

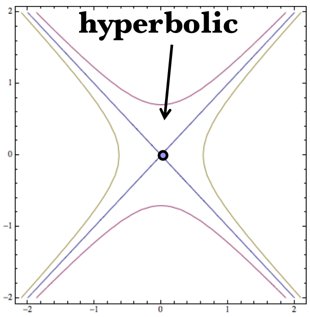

Pendulum fixed point analysis

- The "fixed" points for a pendulum can be found at

$$(\phi_n, p_\phi) = (\pm n\pi, 0) \ , \ n = 0, 1, 2 \ldots$$

- The Jacobian matrix is $\begin{bmatrix} 0 & 1 \\ -\frac{g}{L}\cos\phi_n & 0 \end{bmatrix}$
- The eigenvalues are $\lambda_{1,2} = \pm i\sqrt{\frac{g}{L}\cos\phi_n}$
- Two cases can be distinguished:
  - $\phi_n = 2n\pi$, for which $\lambda_{1,2} = \pm i\sqrt{\frac{g}{L}}$ corresponding to elliptic fixed points
  - $\phi_n = (2n+1)\pi$, for which $\lambda_{1,2} = \pm\sqrt{\frac{g}{L}}$ corresponding to hyperbolic fixed points
  - The **separatrix** are the stable and unstable manifolds passing through the hyperbolic points, separating bounded **librations** and unbounded **rotations**

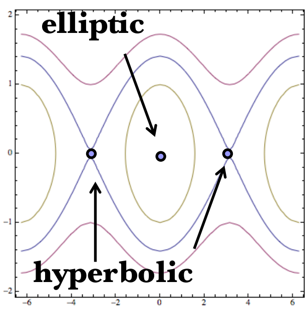

Phase space for time-dependent systems

- Consider now a simple harmonic oscillator where the frequency is time-dependent

$$H = \frac{1}{2}\left(p_u^2 + \omega_0^2(t)u^2\right)$$

- Plotting the evolution in phase space, provides trajectories that intersect each other (top)
- The phase space has time as extra dimension,
- By rescaling the time to become $\tau = \omega_0 t$ and considering every integer interval of the new time variable, the phase space looks like the one of the harmonic oscillator (middle)
- This is the simplest version of a **Poincaré surface of section**, which is useful for studying geometrically phase space of multi-dimensional systems
- The fixed point in the surface of section is now a periodic orbit (bottom)

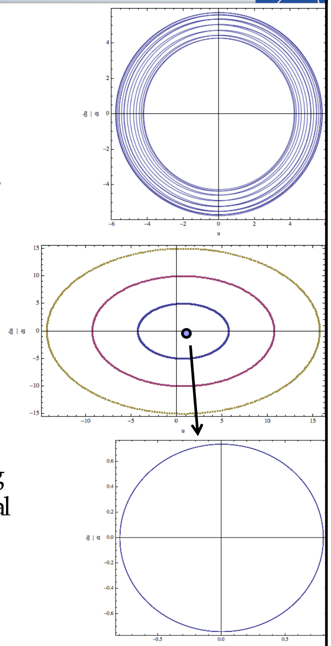

Poincaré Section in practice

- Record the particle coordinates at one location (BPM)
- Unperturbed motion lies on a circle in normalized coordinates (simple rotation)

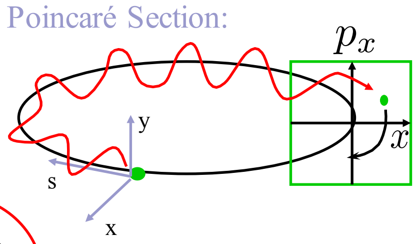

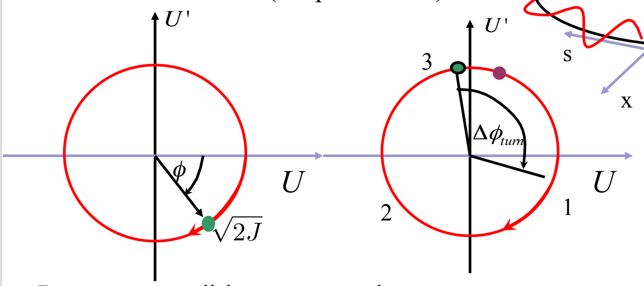

- Resonance condition corresponds to a periodic orbit or in fixed points in phase space
- For a nonliner kick, the radius will change by $\delta(\sqrt{2J})$ and the particles stop lying on circles

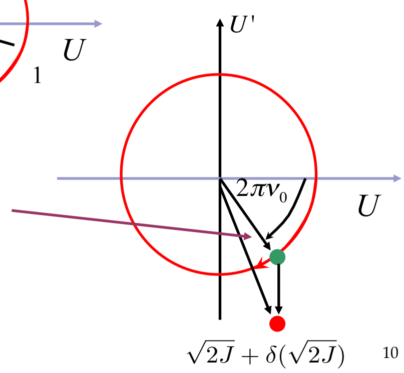

Motion close to a resonance

Secular perturbation theory

- The vicinity of a resonance $n_1\omega_1 + n_2\omega_2 = 0$ can be studied through secular perturbation theory (see appendix)
- A canonical transformation is applied such that the new variables are in a frame remaining on top of the resonance
- If one frequency is slow, one can average the motion and remain only with a 1 degree of freedom Hamiltonian
- Finding the location of the fixed points (J_{10}, ϕ_{10}) (i.e. periodic orbits) in phase space (J_1, ϕ_1) and defining a new action

$\Delta J_1 = J_1 - J_{10}$, the resonant Hamiltonian is

$$H_r(\Delta J_1, \phi_1) = \left.\frac{\partial^2 H_0(\mathbf{J})}{\partial {J_1}^2}\right|_{J_1=J_{10}} \frac{(\Delta J_1)^2}{2} + 2\varepsilon \bar{H}_{n_1,-n_2}(\mathbf{J}) \cos\varphi_1$$

- This is a pendulum where the frequency and the resonance half width are

$$\omega_1 = \left(2\varepsilon H_{n_1,-n_2}(\mathbf{J}) \left.\frac{\partial^2 H_0(\mathbf{J})}{\partial {J_1}^2}\right|_{J_1=J_{10}}\right)^{1/2} \qquad \Delta J_{1\ max} = 2\left(\frac{2\varepsilon H_{n_1,-n_2}(\mathbf{J})}{\left.\frac{\partial^2 H_0(\mathbf{J})}{\partial {J_1}^2}\right|_{J_1=J_{10}}}\right)^{1/2}$$

Secular perturbation theory for the 3rd order resonance

- We first introduce the distance to the resonance

$$\nu = \frac{p}{3} + \delta\,, \quad \delta << 1$$

- It is convenient then to eliminate the "time" dependence by passing on a "1-turn" frame, using the generating function

$$F_2(\phi, J_1, s) = \phi J_1 + J_1 \left(\frac{2\pi\nu s}{C} - \int_0^s \frac{ds'}{\beta(s')} \right) = (\phi + \chi(s)) J_1$$

with the new angle $\psi_1 = \phi - \chi(s)$ providing the Hamiltonian

$$H_1 = \frac{\nu}{R} J_1 + \frac{2\sqrt{2}}{3} K_s(s) (J_1 \beta)^{3/2} \cos^3(\psi_1 + \chi(s))$$

- The perturbation can be expanded in a Fourier series, where only the resonant term is kept or,

$$\hat{H}_1 = \nu J_1 + J_1^{3/2} A_{3p} \cos(3\psi_1 - p\theta)$$

in the rotating frame on top of the resonance

$$\hat{H}_2 = \delta J_2 + J_2^{3/2} A_{3p} \cos(3\psi_2)$$

Fixed points for 3rd order resonance

- By setting the Hamilton's equations equal to zero, three fixed points can be found at $\psi_{20} = \frac{\pi}{3}\,, \ \frac{3\pi}{3}\,, \ \frac{5\pi}{3}\,, \quad J_{20} = \left(\frac{2\delta}{3A_{3p}}\right)^2$
- For $\frac{\delta}{A_{3p}} > 0$ all three points are unstable
- Close to the elliptic one at $\psi_{20} = 0$ the motion in phase space is described by circles that they get more and more distorted to end up in the "triangular" separatrix uniting the unstable fixed points
- The tune separation from the resonance (**stop-band width**) is $\delta = \frac{3A_{3p}}{2} J_{20}^{1/2}$

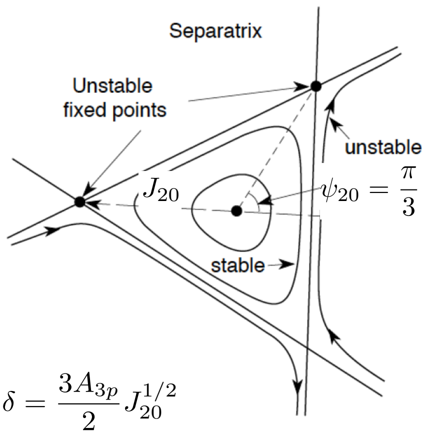

Fixed points for general multi-pole

- For any polynomial perturbation of the form x^k the "resonant" Hamiltonian is written as

$$\hat{H}_2 = \delta J_2 + \alpha(J_2) + J_2^{k/2} A_{kp} \cos(k\psi_2)$$

- Note now that in contrast to the sextupole there is a non-linear detuning term $\alpha(J_2)$
- The conditions for the fixed points are

$$\sin(k\psi_2) = 0 \ , \quad \delta + \frac{\partial\alpha(J_2)}{\partial J_2} + \frac{k}{2} J_2^{k/2-1} A_{kp} \cos(k\psi_2) = 0$$

- There are k fixed points for which $\cos(k\psi_{20}) = -1$ and the fixed points are stable (elliptic). They are surrounded by ellipses
- There are also k fixed points for which $\cos(k\psi_{20}) = 1$ and the fixed points are unstable (hyperbolic). The trajectories are hyperbolas

Fixed points for an octupole

- The resonant Hamiltonian close to the 4th order resonance is written as

$$\hat{H}_2 = \delta J_2 + c J_2^2 + J_2^2 A_{kp} \cos(4\psi_2)$$

- The fixed points are found by taking the derivative over the two variables and setting them to zero, i.e.

$$\sin(4\psi_2) = 0 \ , \quad \delta + 2cJ_2 + 2J_2 A_{kp} \cos(4\psi_2) = 0$$

- The fixed points are at

$$\psi_{20} = \frac{\pi}{4}, \frac{\pi}{2}, \frac{3\pi}{4}, \pi, \frac{5\pi}{4}, \frac{3\pi}{2}, \frac{7\pi}{4}, 2\pi$$

- For half of them, there is a minimum in the potential as $\cos(4\psi_{20}) = -1$ and they are elliptic and half of them they are hyperbolic as $\cos(4\psi_{20}) = 1$

Topology of an octupole resonance

- Regular motion near the center, with curves getting more deformed towards a rectangular shape
- The separatrix passes through 4 unstable fixed points, but motion seems well contained
- Four stable fixed points exist and they are surrounded by stable motion (islands of stability)
- Question: Can the central fixed point become hyperbolic (answer in the appendix)

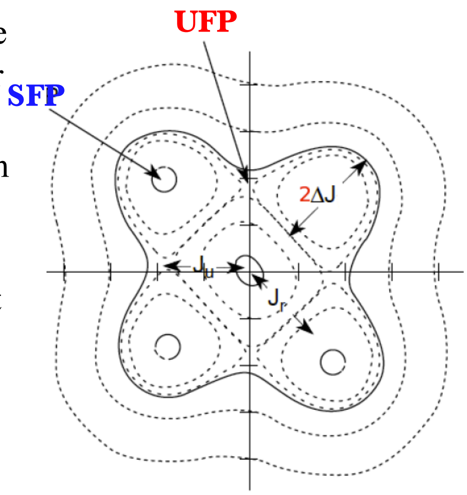

Onset of chaos

Path to chaos

- When perturbation becomes higher, motion around the separatrix becomes chaotic (producing tongues or splitting of the separatrix)
- Unstable fixed points are indeed the source of chaos when a perturbation is added

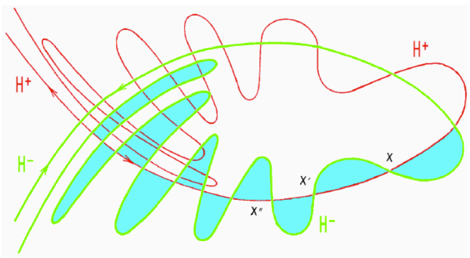

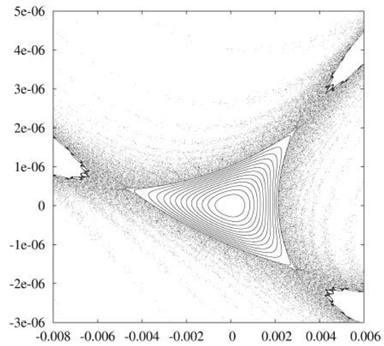

Chaotic motion

- Poincare-Birkhoff theorem states that under perturbation of a resonance only an even number of fixed points survives (half stable and the other half unstable)
- Themselves get destroyed when perturbation gets higher, etc. (self-similar fixed points)
- Resonance islands grow and resonances can overlap allowing diffusion of particles

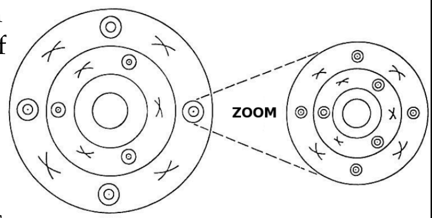

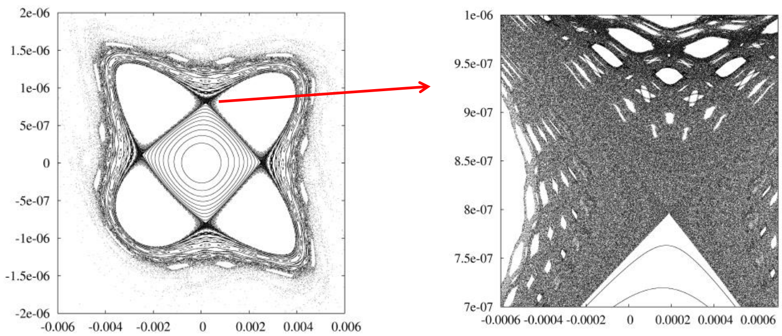

Resonance overlap criterion

- When perturbation grows, the resonance island width grows
- **Chirikov** (1960, 1979) proposed a criterion for the overlap of two neighboring resonances and the onset of orbit diffusion
- The distance between two resonances is $\delta \hat{J}_{1\ n,n'} = \dfrac{2\left(\frac{1}{n_1+n_2} - \frac{1}{n_1'+n_2'}\right)}{\left|\frac{\partial^2 \hat{H}_0(\hat{\mathbf{J}})}{\partial \hat{J}_1^2}\Big|_{\hat{J}_1=\hat{J}_{10}}\right|}$
- The simple overlap criterion is
  $\Delta \hat{J}_{n\ max} + \Delta \hat{J}_{n'\ max} \geq \delta \hat{J}_{n,n'}$
- Considering the width of chaotic layer and secondary islands, the "two thirds" rule apply $\Delta \hat{J}_{n\ max} + \Delta \hat{J}_{n'\ max} \geq \frac{2}{3}\delta \hat{J}_{n,n'}$
- The main limitation is the geometrical nature of the criterion (difficulty to be extended for >2 degrees of freedom)

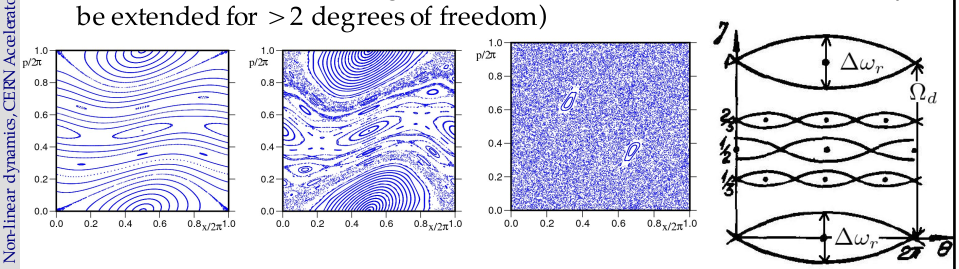

Chaos detection methods

- Computing/measuring dynamic aperture (DA) or particle survival

  A. Chao et al., PRL 61, 24, 2752, 1988;
  F. Willeke, PAC95, 24, 109, 1989.

- Computation of Lyapunov exponents

  F. Schmidt, F. Willeke and F. Zimmermann, PA, 35, 249, 1991;
  M. Giovannozi, W. Scandale and E. Todesco, PA 56, 195, 1997

- Variance of unperturbed action (a la Chirikov)

  B. Chirikov, J. Ford and F. Vivaldi, AIP CP-57, 323, 1979
  J. Tennyson, SSC-155, 1988;
  J. Irwin, SSC-233, 1989

- Fokker-Planck diffusion coefficient in actions

  T. Sen and J.A. Elisson, PRL 77, 1051, 1996

- **Frequency map analysis**

The CERN Accelerator School

Dynamic aperture

The CERN Accelerator School

Dynamic Aperture

- The most direct way to evaluate the non-linear dynamics performance of a ring is the computation of **Dynamics Aperture**
- Particle motion due to multi-pole errors is generally non-bounded, so chaotic particles can **escape to infinity**
- This is not true for all non-linearities (e.g. the beam-beam force)
- Need a **symplectic** tracking code to follow particle trajectories (a lot of initial conditions) for a **number of turns** (depending on the given problem) until the particles start getting lost
- As multi-pole errors may not be completely known, one has to track through **several machine models** built by **random distribution** of these errors
- One could start with 4D (only transverse) tracking but certainly needs to simulate 5D (constant energy deviation) and finally 6D (synchrotron motion included)

Dynamic Aperture plots

- Dynamic aperture plots show the maximum initial values of stable trajectories in x-y coordinate space at a particular point in the lattice, for a range of energy errors.
  - The beam size (injected or equilibrium) can be shown on the same plot.
  - Generally, the goal is to allow some significant margin in the design - the measured dynamic aperture is often smaller than the predicted dynamic aperture.

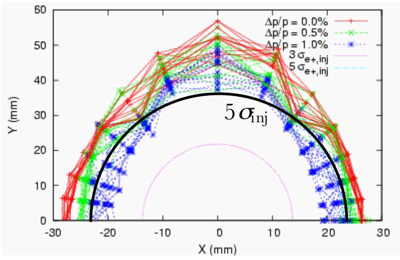

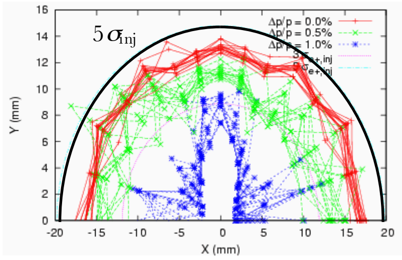

Dynamic aperture including damping

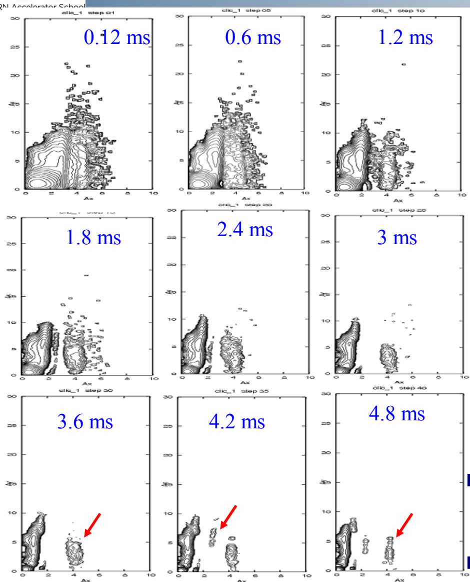

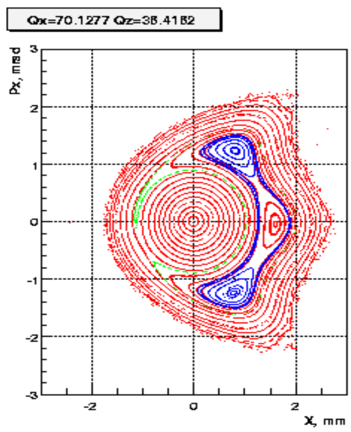

- Including radiation damping and excitation shows that 0.7% of the particles are lost during the damping
- Certain particles seem to damp away from the beam core, on resonance islands

Genetic Algorithms for lattice optimisation

- MOGA –Multi Objective Genetic Algorithms are being recently used to optimise linear but also non-linear dynamics of electron low emittance storage rings
- Use knobs quadrupole strengths, chromaticity sextupoles and correctors with some constraints
- Target ultra-low horizontal emittance, increased lifetime and high dynamic aperture

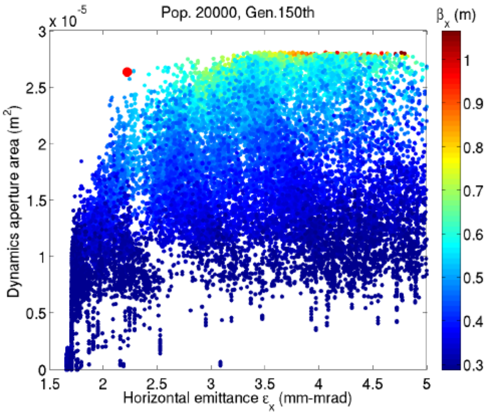

Non-linear dynamics, CERN Accelerator School, October 2015

Measuring Dynamic Aperture

- During LHC design phase DA target was 2x higher than collimator position, due to statistical fluctuation, finite mesh, linear imperfections, short tracking time, multi-pole time dependence, ripple and a 20% safety margin
- Better knowledge of the model led to good agreement between measurements and simulations for actual LHC
- Necessity to build an accurate magnetic model (from beam based measurements)

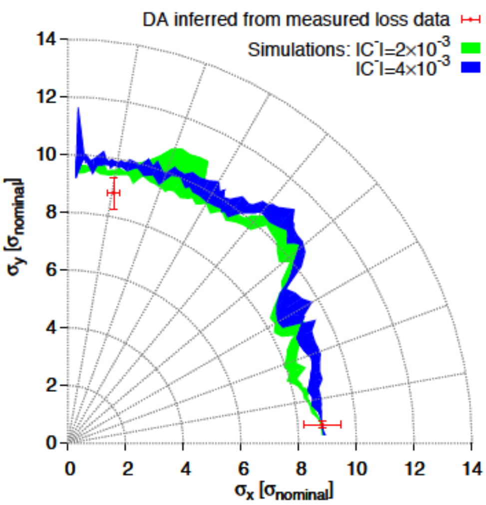

Non-linear dynamics, CERN Accelerator School, October 2015

Frequency Map Analysis

Frequency map analysis

- Frequency Map Analysis (FMA) is a numerical method which springs from the studies of J. Laskar (Paris Observatory) putting in evidence the
- chaotic motion in the Solar Systems
- FMA was successively applied to several dynamical systems
  - Stability of Earth Obliquity and climate stabilization (Laskar, Robutel, 1993)
  - 4D maps (Laskar 1993)
  - Galactic Dynamics (Y.P and Laskar, 1996 and 1998)
  - Accelerator beam dynamics: lepton and hadron rings (Dumas, Laskar, 1993, Laskar, Robin, 1996, Y.P, 1999, Nadolski and Laskar 2001)

Motion on torus

- Consider an integrable Hamiltonian system of the usual form

$$H(\boldsymbol{J}, \boldsymbol{\varphi}, \theta) = H_0(\mathbf{J})$$

- Hamilton's equations give $\dot{\phi}_j = \frac{\partial H_0(\mathbf{J})}{\partial J_j} = \omega_j(\mathbf{J}) \Rightarrow \phi_j = \omega_j(\mathbf{J})t + \phi_{j0}$

$$\dot{J}_j = -\frac{\partial H_0(\mathbf{J})}{\partial \phi_j} = 0 \Rightarrow J_j = \text{const.}$$

- The actions define the surface of an invariant torus
- In complex coordinates the motion is described by

$$\zeta_j(t) = J_j(0)e^{i\omega_j t} = z_{j0}e^{i\omega_j t}$$

- For a **non-degenerate** system $\det\left|\frac{\partial \omega(J)}{\partial J}\right| = \det\left|\frac{\partial^2 H_0(J)}{\partial J^2}\right| \neq 0$ there is a one-to-one correspondence between the actions and the frequency, a frequency map can be defined parameterizing the tori in the frequency space

$$F: \quad (\mathbf{I}) \longrightarrow (\omega)$$

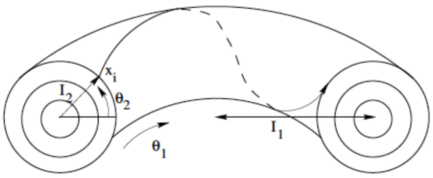

Quasi-periodic motion

- If a transformation is made to some new variables

$$\zeta_j = I_j e^{i\theta_j t} = z_j + \epsilon G_j(\mathbf{z}) = z_j + \epsilon \sum_{\mathbf{m}} c_{\mathbf{m}} z_1^{m_1} z_2^{m_2} \dots z_n^{m_n}$$

- The system is still integrable but the tori are distorted
- The motion is then described by

$$\zeta_j(t) = z_{j0}e^{i\omega_j t} + \sum_{\mathbf{m}} a_{\mathbf{m}} e^{i\,(\mathbf{m}\cdot\omega)\,t}$$

i.e. a **quasi-periodic** function of time, with

$$a_{\mathbf{m}} = \epsilon\, c_{\mathbf{m}} z_{10}^{m_1} z_{20}^{m_2} \dots z_{n0}^{m_n} \text{ and } \mathbf{m}\cdot\omega = m_1\omega_1 + m_2\omega_2 + \dots + m_n\omega_n$$

- For a non-integrable Hamiltonian, $H(\mathbf{I}, \theta) = H_0(\mathbf{I}) + \epsilon H'(\mathbf{I}, \theta)$ and especially if the perturbation is small, most tori persist (**KAM** theory)
- In that case, the motion is still quasi-periodic and a frequency map can be built
- The regularity (or not) of the map reveals stable (or chaotic) motion

Building the frequency map

- When a quasi-periodic function $f(t) = q(t) + ip(t)$ in the complex domain is given numerically, it is possible to recover a quasi-periodic approximation

$$f'(t) = \sum_{k=1}^{N} a'_k e^{i\omega'_k t}$$

in a very precise way over a finite time span $[-T, T]$ several orders of magnitude more precisely than simple Fourier techniques

- This approximation is provided by the Numerical Analysis of Fundamental Frequencies – **NAFF** algorithm
- The frequencies ω'_k and complex amplitudes a'_k are computed through an iterative scheme.

The NAFF algorithm

- The first frequency ω'_1 is found by the location of the maximum of

$$\phi(\sigma) = \langle f(t), e^{i\sigma t} \rangle = \frac{1}{2T} \int_{-T}^{T} f(t) e^{-i\sigma t} \chi(t) dt$$

where $\chi(t)$ is a weight function

- In most of the cases the Hanning window filter is used $\chi_1(t) = 1 + \cos(\pi t/T)$
- Once the first term $e^{i\omega'_1 t}$ is found, its complex amplitude a'_1 is obtained and the process is restarted on the remaining part of the function

$$f_1(t) = f(t) - a'_1 e^{i\omega'_1 t}$$

- The procedure is continued for the number of desired terms, or until a required precision is reached

Frequency determination

- The accuracy of a simple FFT even for a simple sinusoidal signal is not better than $|\nu - \nu_T| = \dfrac{1}{T}$
- Calculating the Fourier integral explicitly

$$\phi(\omega) = < f(t),\ e^{i\omega t} > = \frac{1}{T}\int_0^T f(t)\ e^{-i\omega t}\ dt$$

shows that the maximum lies in between the main picks of the FFT

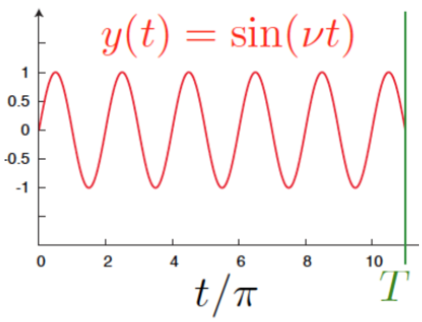

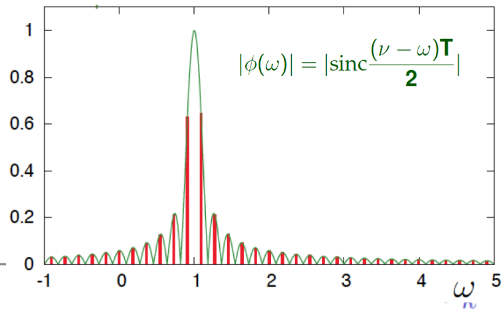

Frequency determination

- A more complicated signal with two frequencies

$$f(t) = a_1 e^{i\omega_1 t} + a_2 e^{i\omega_2 t}$$

shifts slightly the maximum with respect to its real location

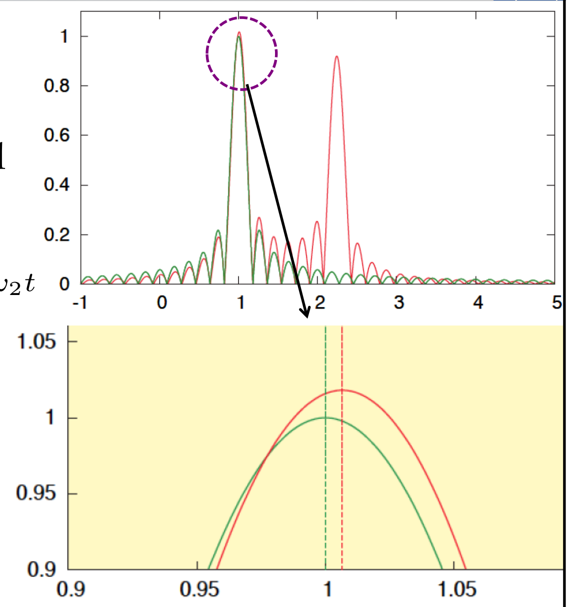

Window function

- A window function like the Hanning filter $\chi_1(t) = 1 + \cos(\pi t/T)$ kills side-lobs and allows a very accurate determination of the frequency

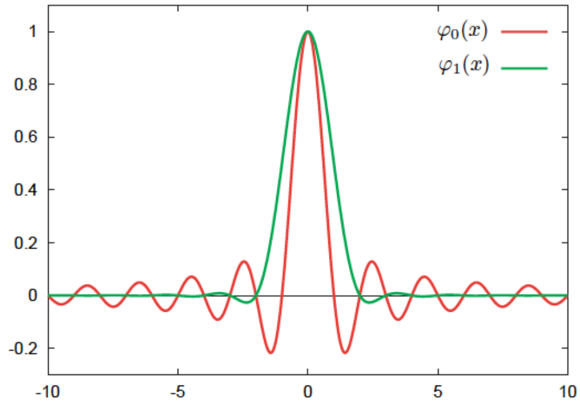

Precision of NAFF

- For a general window function of order p

$$\chi_p(t) = \frac{2^p (p!)^2}{(2p)!}(1 + \cos \pi t)^p$$

Laskar (1996) proved a theorem stating that the solution provided by the NAFF algorithm converges asymptotically towards the real KAM quasi-periodic solution with precision

$$\nu_1 - \nu_1^T \propto \frac{1}{T^{2p+2}}$$

- In particular, for no filter (i.e. $p = 0$) the precision is $\frac{1}{T^2}$, whereas for the Hanning filter ($p = 1$), the precision is of the order of $\frac{1}{T^4}$

Aspects of the frequency map

- In the vicinity of a resonance the system behaves like a pendulum
- Passing through the elliptic point for a fixed angle, a fixed frequency (or rotation number) is observed
- Passing through the hyperbolic point, a frequency jump is oberved

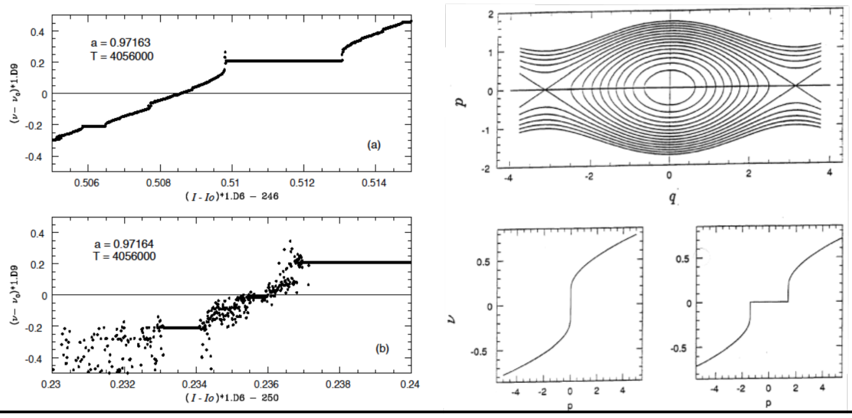

Diffusion in frequency space

- For a 2 degrees of freedom Hamiltonian system, the frequency space is a line, the tori are dots on this lines, and the chaotic zones are confined by the existing KAM tori
- For a system with 3 or more degrees of freedom, KAM tori are still represented by dots but do not prevent chaotic trajectories to diffuse
- This topological possibility of particles diffusing is called **Arnold diffusion**
- This diffusion is supposed to be extremely small in their vicinity, as tori act as effective barriers (**Nechoroshev theory**)

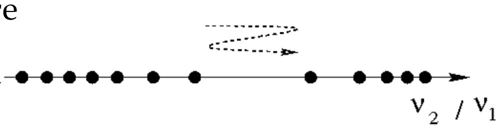

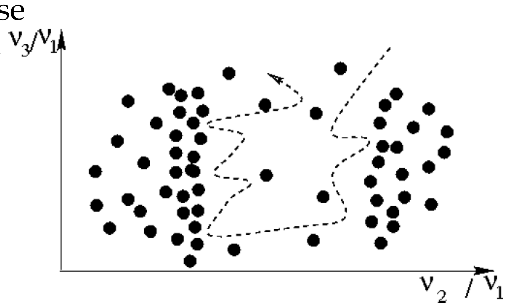

Building the frequency map

- Choose initial conditions (x_i, y_i) with $(p_{x;i}, p_{y;i})$
- Numerically integrate trajectories for sufficient number of turns
- Compute through NAFF $(Q_{x;i}, Q_{y;i})$ after sufficient number of turns
- Plot them in the tune diagram

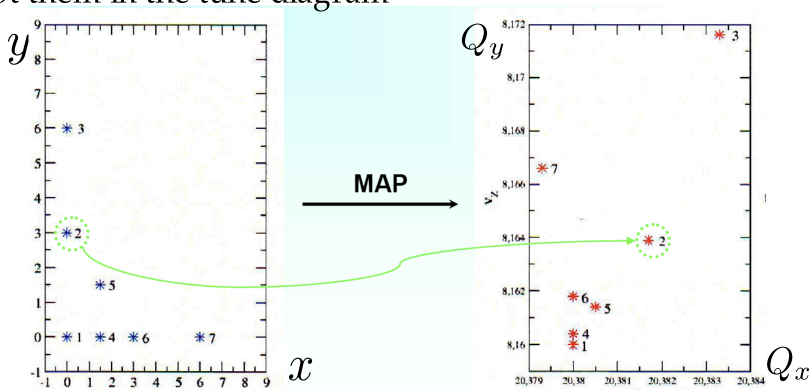

Frequency maps for the LHC

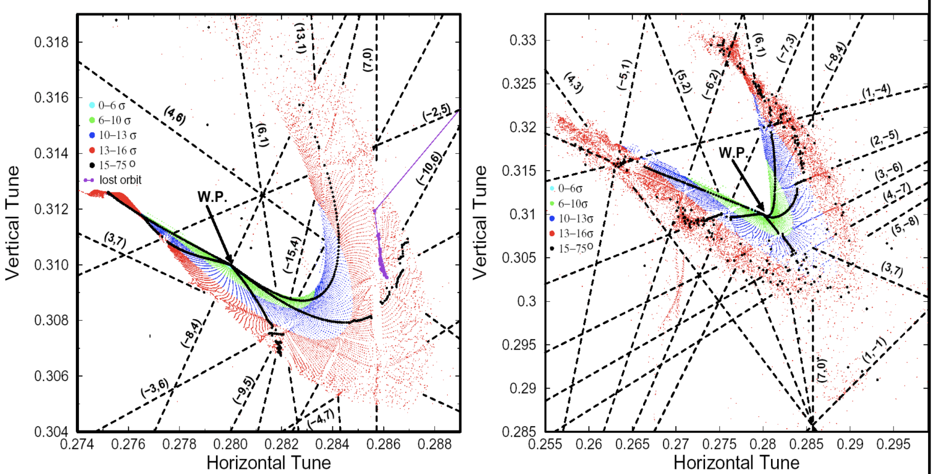

- Frequency maps for the target error table (left) and an increased random skew octupole error in the super-conducting dipoles (right)

Diffusion Maps

- Calculate frequencies for two equal and successive time spans and compute frequency diffusion vector:

$$\boldsymbol{D}\big|_{t=\tau} = \boldsymbol{\nu}\big|_{t\in(0,\tau/2]} - \boldsymbol{\nu}\big|_{t\in(\tau/2,\tau]}$$

- Plot the initial condition space color-coded with the norm of the diffusion vector
- Compute a diffusion quality factor by averaging all diffusion coefficients normalized with the initial conditions radius

$$D_{QF} = \left\langle \frac{|\boldsymbol{D}|}{(I_{x0}^2 + I_{y0}^2)^{1/2}} \right\rangle_R$$

Diffusion maps for the LHC

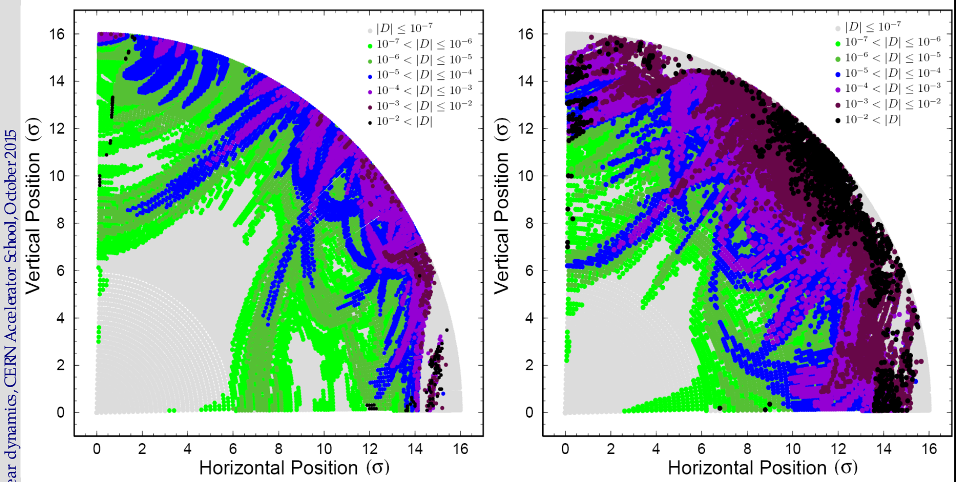

Diffusion maps for the target error table (left) and an increased random skew octupole error in the super-conducting dipoles (right)

Numerical Applications

The CERN Accelerator School

Non-linear dynamics, CERN Accelerator School, October 2015

Correction schemes efficiency

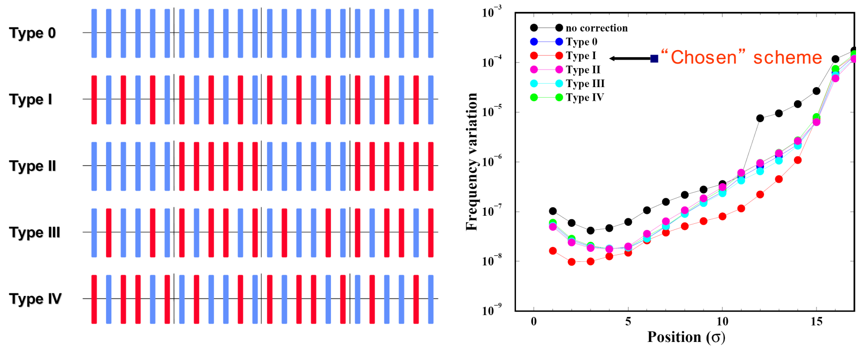

- Comparison of correction schemes for b_4 and b_5 errors in the LHC dipoles
- Frequency maps, resonance analysis, tune diffusion estimates, survival plots and short term tracking, proved that only half of the correctors are needed

Beam-Beam interaction

Variable	Symbol	Value
Beam energy	E	7 TeV
Particle species	$\cdots$	protons
Full crossing angle	θ_c	300 μrad
rms beam divergence	σ'_x	31.7 μrad
rms beam size	σ_x	15.9 μm
Normalized transv. rms emittance	$\gamma\varepsilon$	3.75 μm
IP beta function	β^*	0.5 m
Bunch charge	N_b	$(1\times10^{11}$–$2\times10^{12})$
Betatron tune	Q_0	0.31

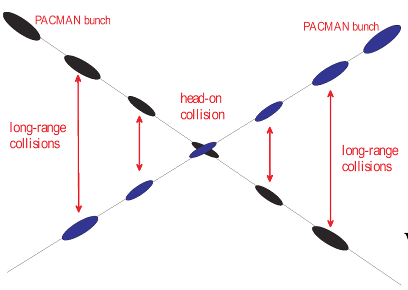

- Long range beam-beam interaction represented by a 4D kick-map

$$\Delta x = -\, n_{par} \frac{2 r_p N_b}{\gamma} \left[\frac{x' + \theta_c}{\theta_t^2} \left(1 - e^{-\frac{\theta_t^2}{2\theta_{x,y}^2}} \right) - \frac{1}{\theta_c} \left(1 - e^{-\frac{\theta_c^2}{2\theta_{x,y}^2}} \right) \right]$$

$$\Delta y = -\, n_{par} \frac{2 r_p N_b}{\gamma} \frac{y'}{\theta_t^2} \left(1 - e^{-\frac{\theta_t^2}{2\theta_{x,y}^2}} \right)$$

with $\quad \theta_t \equiv \left((x' + \theta_c)^2 + y'^2 \right)^{1/2}$

Non-linear dynamics, CERN Accelerator School, October 2015

47

Head-on vs Long range interaction

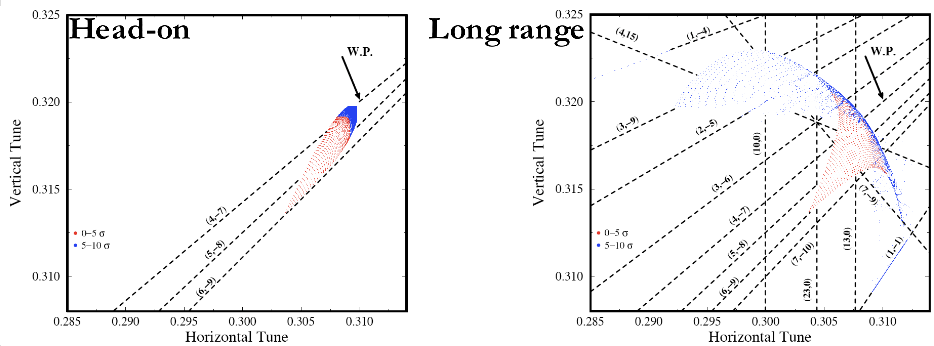

- Proved dominant effect of long range beam-beam effect
- Dynamics dominated by the 1/r part of the force, reproduced by electrical wire, which was proposed for correcting the effect
- Experimental verification in SPS and installation to the LHC IPs

Non-linear dynamics, CERN Accelerator School, October 2015

48

Action variance vs. frequency diffusion

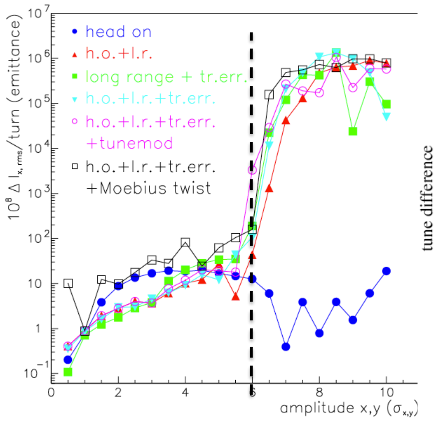

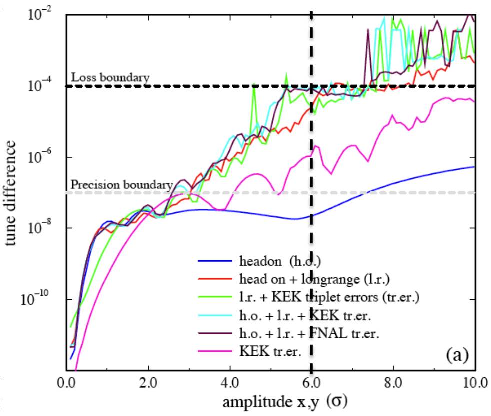

- Very good agreement of diffusive aperture boundary (action variance) with frequency variation (loss boundary corresponding to around 1 integer unit change in 10^7 turns)

Magnet fringe fields

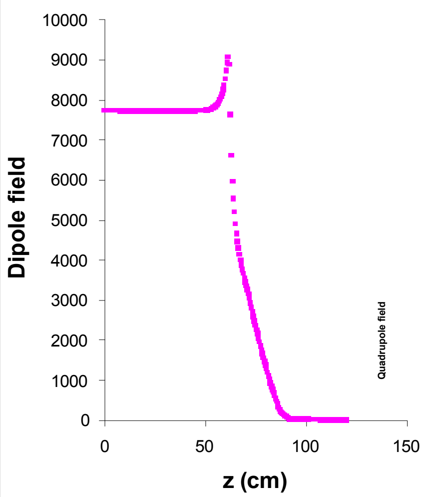

- Up to now we considered only transverse fields
- Magnet fringe field is the longitudinal dependence of the field at the magnet edges
- Important when magnet aspect ratios and/or emittances are big

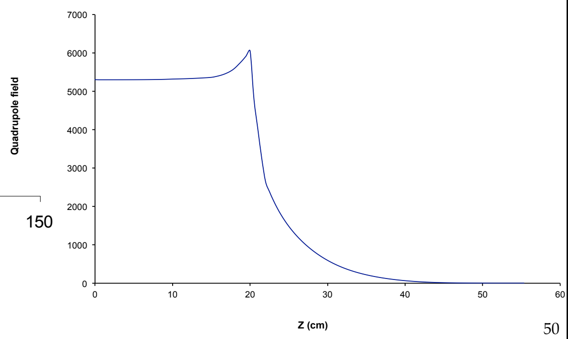

Quadrupole fringe field

General field expansion for a quadrupole magnet:

$$B_x = \sum_{m,n=0}^{\infty} \sum_{l=0}^{m} \frac{(-1)^m x^{2n} y^{2m+1}}{(2n)!(2m+1)!} \binom{m}{l} b^{[2l]}_{2n+2m+1-2l}$$

$$B_y = \sum_{m,n=0}^{\infty} \sum_{l=0}^{m} \frac{(-1)^m x^{2n+1} y^{2m}}{(2n+1)!(2m)!} \binom{m}{l} b^{[2l]}_{2n+2m+1-2l} \quad .$$

$$B_z = \sum_{m,n=0}^{\infty} \sum_{l=0}^{m} \frac{(-1)^m x^{2n+1} y^{2m+1}}{(2n+1)!(2m+1)!} \binom{m}{l} b^{[2l+1]}_{2n+2m+1-2l}$$

and to leading order

$$\begin{aligned} B_x &= y\left[b_1 - \frac{1}{12}(3x^2+y^2)b_1^{[2]}\right] + O(5) \\ B_y &= x\left[b_1 - \frac{1}{12}(3y^2+x^2)b_1^{[2]}\right] + O(5) \\ B_z &= xyb_1^{[1]} + O(4) \end{aligned}$$

The quadrupole fringe to leading order has an octupole-like effect

Magnet fringe fields

- From the hard-edge Hamiltonian

$$H_f = \frac{\pm Q}{12B\rho(1+\frac{\delta p}{p})}(y^3 p_y - x^3 p_x + 3x^2 y p_y - 3y^2 x p_x),$$

the first order shift of the frequencies with amplitude can be computed analytically

$$\begin{pmatrix} \delta\nu_x \\ \delta\nu_y \end{pmatrix} = \begin{pmatrix} a_{hh} & a_{hv} \\ a_{hv} & a_{vv} \end{pmatrix} \begin{pmatrix} 2J_x \\ 2J_y \end{pmatrix},$$

with the "anharmonicity" coefficients (torsion)

$$\begin{aligned} a_{hh} &= \frac{-1}{16\pi B\rho} \textstyle\sum_i \pm Q_i \beta_{xi}\alpha_{xi} \\ a_{hv} &= \frac{1}{16\pi B\rho} \textstyle\sum_i \pm Q_i (\beta_{xi}\alpha_{yi} - \beta_{yi}\alpha_{xi}) \\ a_{vv} &= \frac{1}{16\pi B\rho} \textstyle\sum_i \pm Q_i \beta_{yi}\alpha_{yi} \end{aligned}$$

Tune footprint for the SNS based on hard-edge (red) and realistic (blue) quadrupole fringe-field

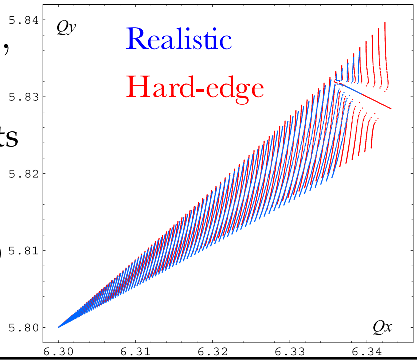

Off-momentum frequency maps

SNS Working Point $(Q_x,Q_y)=(6.4,6.3)$

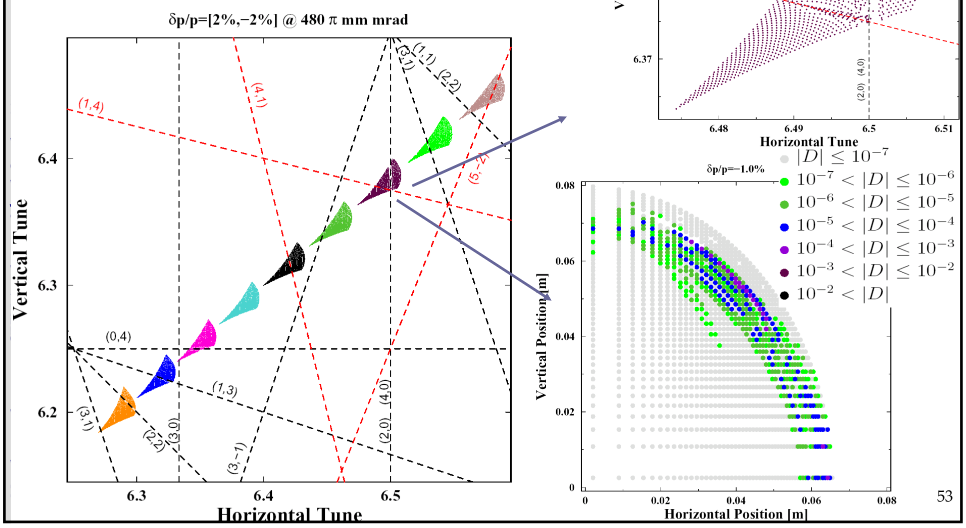

53

Choice of the SNS ring working point

Tune Diffusion quality factor

$$D_{QF} = \left\langle \frac{|D|}{(I_{x0}^2 + I_{y0}^2)^{1/2}} \right\rangle_R$$

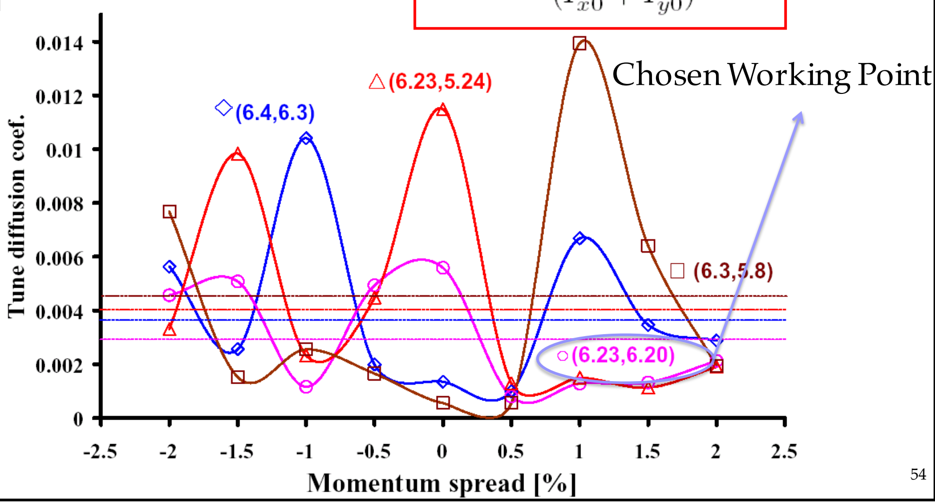

54

Global Working point choice

- Figure of merit for choosing best working point is sum of diffusion rates with a constant added for every lost particle
- Each point is produced after tracking 100 particles
- Nominal working point had to be moved towards "blue" area

$$e^D = \sqrt{\frac{(\nu_{x,1}-\nu_{x,2})^2 + (\nu_{y,1}-\nu_{y,2})^2}{N/2}}$$

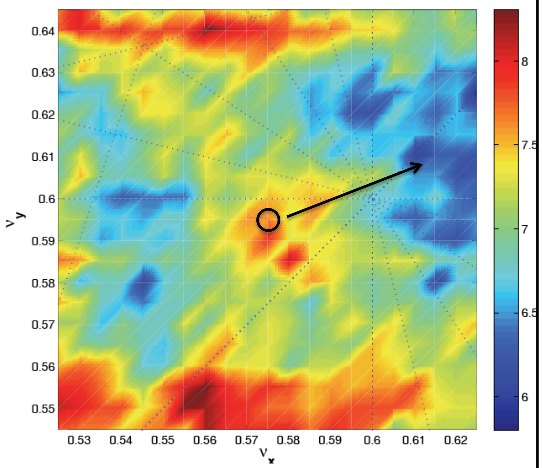

$$WPS = 0.1N_{lost} + \sum e^D$$

Advanced symplectic integration schemes

- Symplectic integrators with **positive** steps for Hamiltonian systems $H = A + \epsilon B$ with both A and B **integrable** were proposed by McLachan (1995).
- Laskar and Robutel (2001) derived all orders of such integrators
- Consider the formal solution of the Hamiltonian system written in the Lie representation

$$\vec{x}(t) = \sum_{n\geq 0} \frac{t^n}{n!} L_H^n \vec{x}(0) = e^{tL_H}\vec{x}(0).$$

- A symplectic integrator of order n from t to $t+\tau$ consists of approximating the Lie map $e^{\tau L_H} = e^{\tau(L_A + L_{\epsilon B})}$ by products of $e^{c_i \tau L_A}$ and $e^{d_i \tau L_{\epsilon B}}$, $i = 1, \ldots, n$ which integrate exactly A and B over the time-spans $c_i\tau$ and $d_i\tau$
- The constants c_i and d_i are chosen to reduce the error

SABA$_2$ integrator

- The SABA$_2$ integrator is written as

$$\mathrm{SABA}_2 = e^{c_1 \tau L_A} e^{d_1 \tau L_{\epsilon B}} e^{c_2 \tau L_A} e^{d_1 \tau L_{\epsilon B}} e^{c_1 \tau L_A},$$

with $c_1 = \frac{1}{2}\left(1 - \frac{1}{\sqrt{3}}\right)$, $c_2 = \frac{1}{\sqrt{3}}$, $d_1 = \frac{1}{2}$.

- When $\{\{A, B\}, B\}$ is integrable, e.g. when A is quadratic in momenta and B depends only in positions, the accuracy of the integrator is improved by two small negative kicks

$$\mathrm{SABA_2C} = e^{-\tau^3 \epsilon^2 \frac{c}{2} L_{\{\{A,B\},B\}}} (\mathrm{SABA}_2)\, e^{-\tau^3 \epsilon^2 \frac{c}{2} L_{\{\{A,B\},B\}}}$$

with $c = (2 - \sqrt{3})/24$

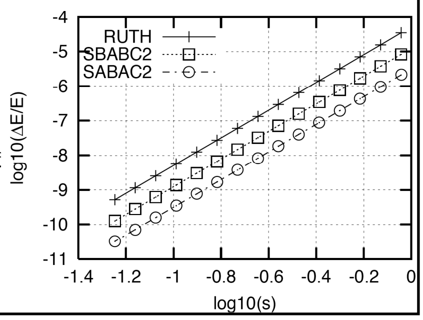

- The accuracy of SABA$_2$C is one order of magnitude higher than the Forest-Ruth 4th order scheme
- The usual "drift-kick" scheme corresponds to the 2nd order inte

$$\mathrm{SABA}_1 = e^{\frac{\tau}{2} L_A} e^{\tau L_{\epsilon B}} e^{\frac{\tau}{2} L_A},$$

Non-linear dynamics, CERN Accelerator School, October 2015

Application of the SABA$_2$C integrator

- The one kick integrator reveals a completely different dynamics then the 10-kick
- SABA$_2$C integrator captures the correct dynamics

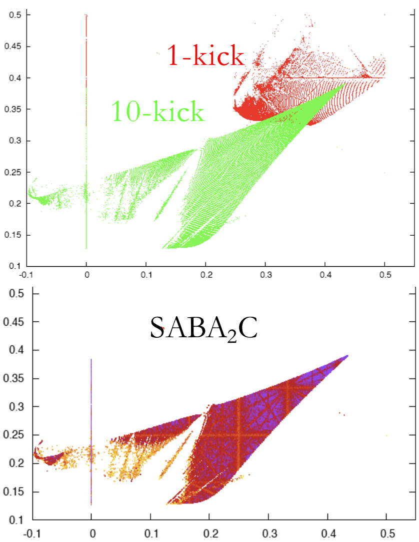

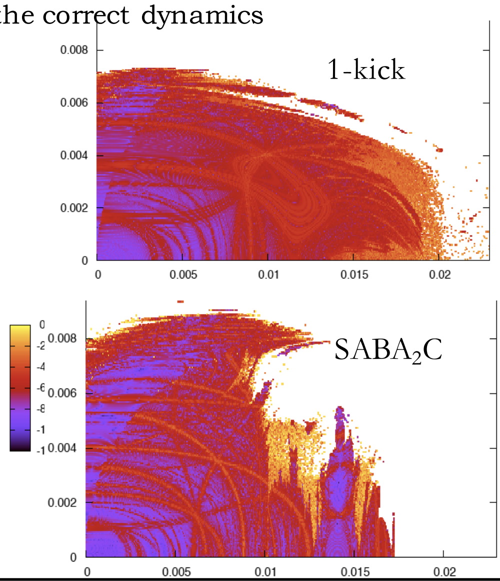

Non-linear dynamics, CERN Accelerator School, October 2015

Sextupole scheme optimization

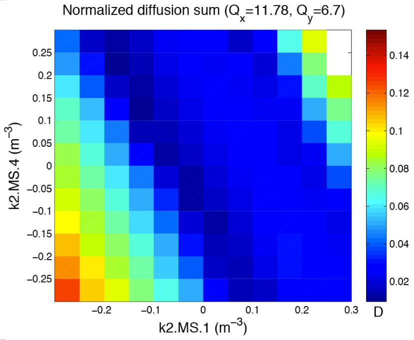

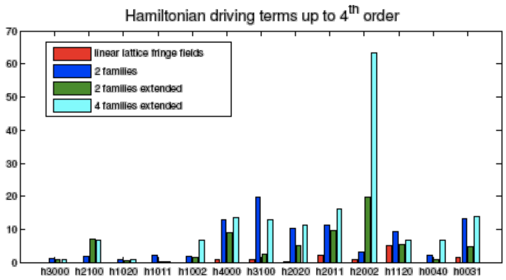

- Comparing different chromaticity sextupole correction schemes and working point optimization using normal form analysis, frequency maps and finally particle tracking
- Finding the adequate sextupole strengths through the tune diffusion coefficient

Experimental methods

Experimental frequency maps

- Frequency analysis of turn-by-turn data of beam oscillations produced by a fast kicker magnet and recorded on a Beam Position Monitors
- Reproduction of the non-linear model of the Advanced Light Source storage ring and working point optimization for increasing beam lifetime

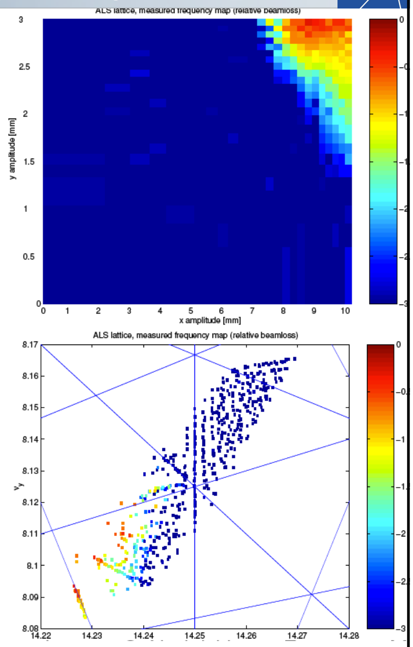

Experimental Methods – Tune scans

- Study the resonance behavior around different working points
- Strength of individual resonance lines can be identified from the beam loss rate, i.e. the derivative of the beam intensity at the moment of crossing the resonance
- Vertical tune is scanned from about 0.45 down to 0.05 during a period (3s) along the flat bottom
- Horizontal tune is constant during the same period
- Tunes are continuously monitored using tune monitor (tune post-processed with NAFF) and the beam intensity is recorded with a beam current transformer

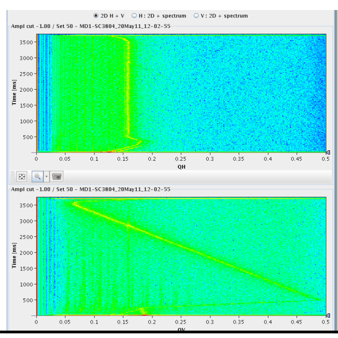

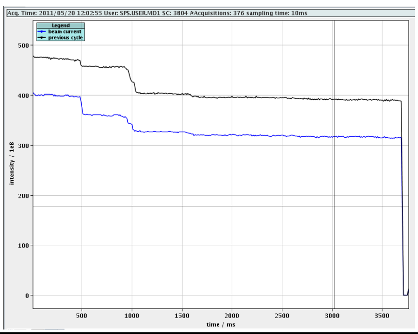

Tune Scans from the SPS

- Plot the tunes color-coded with the amount of loss
- Identify the dangerous resonances
- Compare between two different optics
- Try to refine the machine model

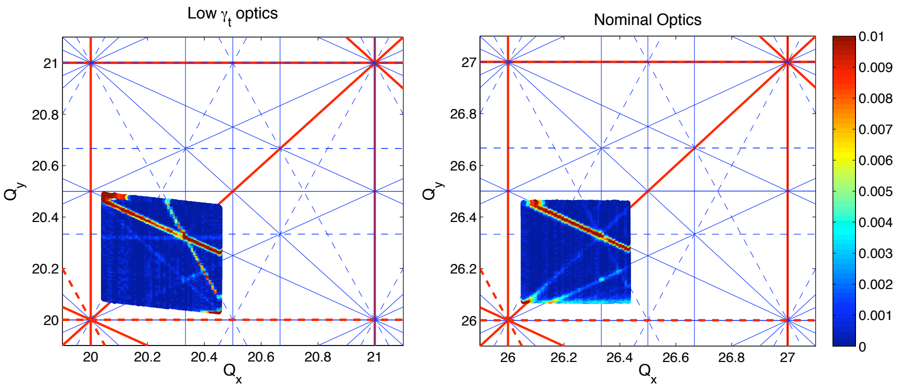

Summary

- **Resonances** (stable and unstable fixed points) are responsible for the onset of **chaos**
- **Dynamic aperture** by brute force tracking (with symplectic numerical integrators) is the usual quality criterion for evaluating non-linear dynamics performance of a machine
- **Frequency Map Analysis** is a numerical tool that enables to study in a global way the dynamics, by identifying the excited **resonances** and the extent of **chaotic** regions
- It can be directly applied to **tracking** but also **experimental** data
- A combination of these modern methods enable a thorough analysis of non-linear dynamics and lead to a robust design

Acknowledgments

Thanks to F.Antoniou, H.Bartosik, W.Herr, J.Laskar, S.Liuzzo, L.Nadolski,D.Robin, C.Skokos, C.Steier, F.Schmidt, A.Wolski, F.Zimmermann

Appendix

The pendulum

- An important non-linear equation which can be integrated is the one of the pendulum, for a string of length L and gravitational constant g

$$\frac{d^2\phi}{dt^2} + \frac{g}{L}\sin\phi = 0$$

- For small displacements it reduces to an harmonic oscillator with frequency $\omega_0 = \sqrt{\frac{g}{L}}$
- The integral of motion (scaled energy) is

$$\frac{1}{2}\left(\frac{d\phi}{dt}\right)^2 - \frac{g}{L}\cos\phi = I_1 = E'$$

and the quadrature is written as $t = \int \frac{d\phi}{\sqrt{2(I_1 + \frac{g}{L}\cos\phi)}}$
assuming that for $t = 0\,, \quad \phi = 0$

Non-linear dynamics, CERN Accelerator School, October 2015

67

Solution for the pendulum

- Using the substitutions $\cos\phi = 1 - 2k^2\sin^2\theta$ with $k = \sqrt{1/2(1 + I_1 L/g)}$, the integral is

$$t = \sqrt{\frac{L}{g}}\int_0^\theta \frac{d\theta}{\sqrt{1 - k^2\sin^2\theta}}$$ and can be solved using

Jacobi elliptic functions: $\phi(t) = 2\arcsin\left[k\ \mathrm{sn}\left(t\sqrt{\frac{g}{L}}, k\right)\right]$

- For recovering the period, the integration is performed between the two extrema, i.e. $\phi = 0$ and $\phi = \arccos(-I_1 L/g)$, corresponding to $\theta = 0$ and $\theta = \pi/2$, for which

$$T = 4\sqrt{\frac{L}{g}}\int_0^{\pi/2} \frac{d\theta}{\sqrt{1 - k^2\sin^2\theta}} = 4\sqrt{\frac{L}{g}}\mathcal{F}(\pi/2, k)$$

i.e. the complete elliptic integral multiplied by four times the period of the harmonic oscillator

Non-linear dynamics, CERN Accelerator School, October 2015

68

Secular perturbation theory

- Consider a general two degrees of freedom Hamiltonian:

$$H(\mathbf{J},\boldsymbol{\varphi}) = H_0(\mathbf{J}) + \varepsilon H_1(\mathbf{J},\boldsymbol{\varphi})$$

with the perturbed part periodic in angles:

$$H_1(\mathbf{J},\boldsymbol{\varphi}) = \sum_{k_1,k_1} H_{k_1,k_2}(J_1,J_2)\exp[i(k_1\varphi_1 + k_2\varphi_2)]$$

- The resonance $n_1\omega_1 + n_2\omega_2 = 0$ prevents the convergence of the series
- A canonical transformation can be applied for eliminating one action: $(\mathbf{J},\boldsymbol{\varphi}) \longmapsto (\hat{\mathbf{J}},\hat{\boldsymbol{\varphi}})$ using the generating function $F_r(\hat{\mathbf{J}},\boldsymbol{\varphi}) = (n_1\varphi_1 - n_2\varphi_2)\hat{J}_1 + \varphi_2\hat{J}_2$
- The relationships between new and old variables are

$$J_1 = n_1\hat{J}_1 \quad , \quad J_2 = \hat{J}_2 - n_2\hat{J}_1$$

$$\hat{\varphi}_1 = n_1\varphi_1 - n_2\varphi_2 \quad , \quad \hat{\varphi}_2 = \varphi_2$$

- This transformation put us in a rotating frame where the rate of change $\dot{\hat{\varphi}}_1 = n_1\dot{\varphi}_1 - n_2\dot{\varphi}_2$ measures the deviation from resonance

Secular perturbation theory

- The transformed Hamiltonian is $\hat{H}(\hat{\mathbf{J}},\hat{\boldsymbol{\varphi}}) = \hat{H}_0(\hat{\mathbf{J}}) + \varepsilon\hat{H}_1(\hat{\mathbf{J}},\hat{\boldsymbol{\varphi}})$ with the perturbation written as a Fourier series

$$\hat{H}_1(\hat{\mathbf{J}},\hat{\boldsymbol{\varphi}}) = \sum_{k_1,k_2} H_{k_1,k_2}(\hat{\mathbf{J}})\exp\left\{\frac{i}{n_1}[k_1\hat{\varphi}_1 + (k_1n_2 + k_2n_1)\hat{\varphi}_1]\right\}$$

- This transformation assumes that $\dot{\hat{\varphi}}_2$ is the slow frequency and we can average the Hamiltonian over the corresponding angle to obtain

$$\bar{H}(\hat{\mathbf{J}},\hat{\boldsymbol{\varphi}}) = \bar{H}_0(\hat{\mathbf{J}}) + \varepsilon\bar{H}_1(\hat{\mathbf{J}},\hat{\varphi}_1) \text{ with } \bar{H}_0(\hat{\mathbf{J}}) = \hat{H}_0(\hat{\mathbf{J}}) \text{ and}$$

$$\bar{H}_1(\hat{\mathbf{J}},\hat{\varphi}_1) = \langle\hat{H}_1(\hat{\mathbf{J}},\hat{\varphi}_1)\rangle_{\hat{\varphi}_2} = \sum_{p=-\infty}^{+\infty} H_{-pn_1,pn_2}(\hat{\mathbf{J}})\exp(-ip\hat{\varphi}_1)$$

- The averaging eliminated one angle and thus $\hat{J}_2 = J_2 + J_1\frac{n_2}{n_1}$ is an invariant of motion
- This means that the Hamiltonian has effectively only one degree of freedom and it is integrable

Secular perturbation theory

- Assuming that the dominant Fourier harmonics for $p = 0, \pm 1$ the Hamiltonian is written as
  $\bar{H}(\hat{\boldsymbol{J}}, \hat{\boldsymbol{\phi}}_1) = \bar{H}_0(\hat{\mathbf{J}}) + \varepsilon \bar{H}_{0,0}(\hat{\mathbf{J}}) + 2\varepsilon \bar{H}_{n_1,-n_2}(\hat{\mathbf{J}}) \cos \hat{\varphi}_1$
- Fixed points $(\hat{J}_{10}, \hat{\phi}_{10})$ (i.e. periodic orbits) in phase space $(\hat{J}_1, \hat{\phi}_1)$ are defined by $\frac{\partial \bar{H}}{\partial \hat{J}_1} = 0\,,\ \frac{\partial \bar{H}}{\partial \hat{\phi}_1} = 0$
- Move the reference on fixed point and expand $\bar{H}(\hat{\mathbf{J}})$ around $\Delta \hat{J}_1 = \hat{J}_1 - \hat{J}_{10}$
- Hamiltonian describing motion near a resonance:

$$\bar{H}_r(\Delta \hat{J}_1, \hat{\phi}_1) = \left.\frac{\partial^2 \bar{H}_0(\hat{\mathbf{J}})}{\partial \hat{J}_1^{\,2}}\right|_{\hat{J}_1 = \hat{J}_{10}} \frac{(\Delta \hat{J}_1)^2}{2} + 2\varepsilon \bar{H}_{n_1,-n_2}(\hat{\mathbf{J}}) \cos \hat{\varphi}_1$$

- Motion near a typical resonance is like the one of the pendulum!!! The frequency and the resonance half width are

$$\hat{\omega}_1 = \left(2\varepsilon \bar{H}_{n_1,-n_2}(\hat{\mathbf{J}}) \left.\frac{\partial^2 \bar{H}_0(\hat{\mathbf{J}})}{\partial \hat{J}_1^{\,2}}\right|_{\hat{J}_1 = \hat{J}_{10}} \right)^{1/2} \qquad \Delta \hat{J}_{1\,max} = 2 \left(\frac{2\varepsilon \bar{H}_{n_1,-n_2}(\hat{\mathbf{J}})}{\left.\frac{\partial^2 \bar{H}_0(\hat{\mathbf{J}})}{\partial \hat{J}_1^{\,2}}\right|_{\hat{J}_1 = \hat{J}_{10}}} \right)^{1/2}$$

Octupole with hyperbolic central fixed point

- Now, if $c = 0$ the solution for the action is $J_{20} = 0$
- So there is no minima in the potential, i.e. the central fixed point is hyperbolic

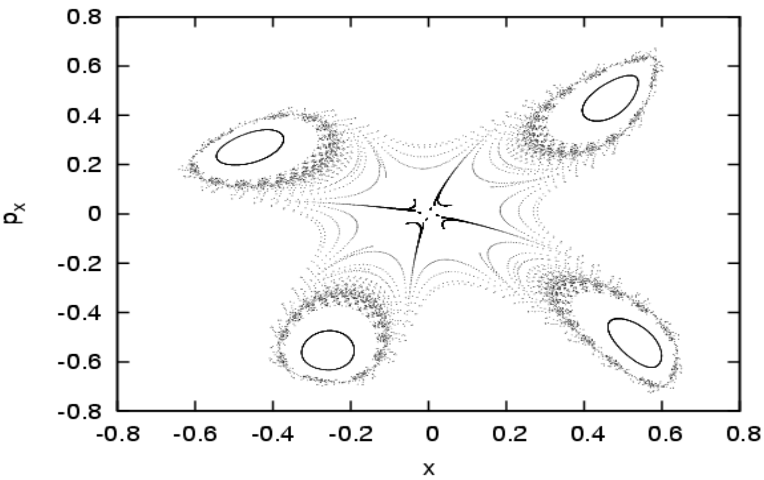

Experimental non-linear dynamics at ESRF

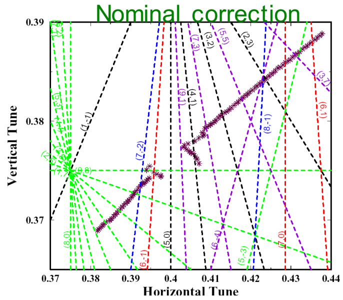

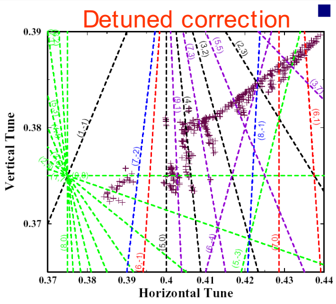

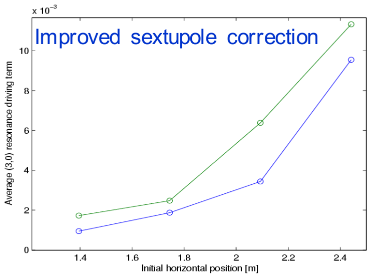

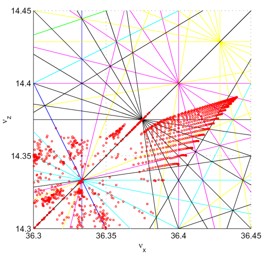

- 3 regions:
  - Small amplitudes: regular motion
  - Medium amplitudes: 5th order resonance crossing
  - Large amplitudes: losses due to 3rd order resonance crossing
- Excitation of 3rd order resonance and correction with sextupole correctors

Resonance free lattice for CLIC PDR

- Non linear optimization based on phase advance scan for minimization of resonance driving terms and tune-shift with amplitude

$$\left|\sum_{p=0}^{N_c-1} e^{ip(n_x\mu_{x,c}+n_y\mu_{y,c})}\right| = \sqrt{\frac{1-\cos\left[N_c(n_x\mu_{x,c}+n_y\mu_{y,c})\right]}{1-\cos(n_x\mu_{x,c}+n_y\mu_{y,c})}} = 0$$

$$\Downarrow$$

$$N_c(n_x\mu_{x,c}+n_y\mu_{y,c}) = 2k\pi$$

$$n_x\mu_{x,c}+n_y\mu_{y,c} \neq 2k'\pi$$

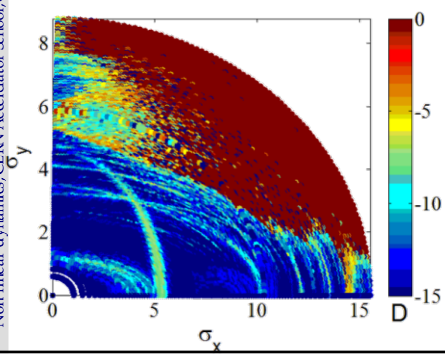

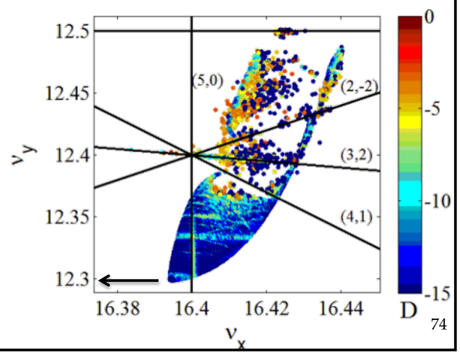

The CERN Accelerator School

Space charge frequency scan

- Injecting high bunch density beam into the SPS
- Space charge effect quite strong with (linear) tune-shifts of
- Changing horizontal/vertical frequency and measuring emittance (action) blow-up

$\Delta Q_x/\Delta Q_y$ ~ 0.10/0.18

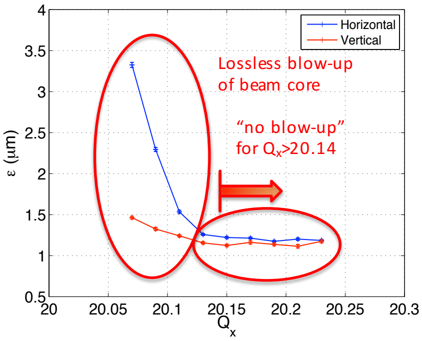

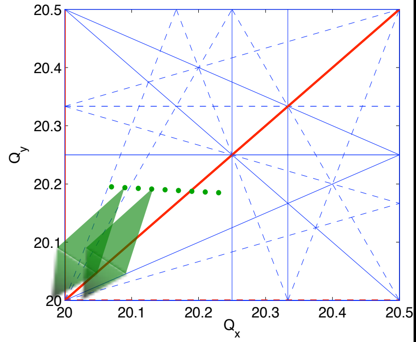

The CERN Accelerator School

Space charge frequency scan

- Injecting high bunch density beam into the SPS
- Space charge effect quite strong with (linear) tune-shifts of
- Changing horizontal/vertical frequency and measuring emittance (action) blow-up

$\Delta Q_x/\Delta Q_y$ ~ 0.10/0.18